3446–3457 *Nucleic Acids Research, 2018, Vol. 46, No. 7* *Published online 13 February 2018*
doi: 10.1093/nar/gky088

Super-resolution imaging identifies PARP1 and the Ku complex acting as DNA double-strand break sensors

Guang Yang[1], Chao Liu[1], Shih-Hsun Chen[1], Muzaffer A. Kassab[1], J. Damon Hoff[2], Nils G. Walter[2,3] and Xiaochun Yu[1,*]

[1]Department of Cancer Genetics and Epigenetics, Beckman Research Institute, City of Hope, Duarte, CA 91010, USA, [2]Single Molecule Analysis in Real-Time (SMART) Center, University of Michigan, Ann Arbor, MI 48109, USA and [3]Single Molecule Analysis Group and Center for RNA Biomedicine, Department of Chemistry, University of Michigan, Ann Arbor, MI 48109, USA

Received November 27, 2017; Revised January 25, 2018; Editorial Decision January 26, 2018; Accepted January 29, 2018

ABSTRACT

DNA double-strand breaks (DSBs) are fatal DNA lesions and activate a rapid DNA damage response. However, the earliest stage of DSB sensing remains elusive. Here, we report that PARP1 and the Ku70/80 complex localize to DNA lesions considerably earlier than other DSB sensors. Using super-resolved fluorescent particle tracking, we further examine the relocation kinetics of PARP1 and the Ku70/80 complex to a single DSB, and find that PARP1 and the Ku70/80 complex are recruited to the DSB almost at the same time. Notably, only the Ku70/80 complex occupies the DSB exclusively in the G1 phase; whereas PARP1 competes with the Ku70/80 complex at the DSB in the S/G2 phase. Moreover, in the S/G2 phase, PARP1 removes the Ku70/80 complex through its enzymatic activity, which is further confirmed by *in vitro* DSB-binding assays. Taken together, our results reveal PARP1 and the Ku70/80 complex as critical DSB sensors, and suggest that PARP1 may function as an important regulator of the Ku70/80 complex at the DSBs in the S/G2 phase.

INTRODUCTION

DNA is the target of both endogenous and exogenous insults that can chingcause serious damage to the genome. DNA DSBs are fatal lesions and must be repaired quickly to prevent random chromosomal recombination events. Once DNA DSBs occur, cells quickly recognize them and amplify the signals to the downstream effectors including cell cycle checkpoints and DNA damage repair machinery (1,2). This quick reaction requires abundant DSB sensors for lesion surveillance and recruitment of effectors which mount a coordinated response to maintain the genomic integrity (3). However, the earliest DSB sensors underlying the primary recognition remain largely elusive.

To date, several DSB sensors have been identified, including the MRN complex, the RPA complex, sirtuins, the Ku complex and PARP1. The MRN complex contains MRE11, RAD50 and NBS1 (4), and is essential for the activation of ATM (5), a major kinase to induce phosphorylation cascade in response to DSBs (6,7). Among these three subunits, RAD50 recognizes the naked DNA ends and holds the ends in close proximity (8); MRE11, an endo and exo-nuclease, processes the DNA ends for re-ligation (9,10); and NBS1 mediates the interactions with other functional partners of the complex (11). The MRN complex is known to be involved in the initial sensing and processing of DSBs (12). However, the MRN complex is not highly abundant within the cell, suggesting that each MRN complex covers a large part of the genome, and may not function as the quickest sensor localized to a DNA lesion because of the low concentration of the complex.

The RPA complex, composed of RPA1, 2 and 3 mediates the activation of ATR in response to DSBs (13). Although the RPA complex is quite abundant in cells, it recognizes only single-stranded DNA that is generated from the processing of DSB ends (14). Thus, similar to the MRN complex, the RPA complex is more likely to act as a late or secondary sensor of DSBs.

The Ku complex is a heterodimer composed of the Ku70 and Ku80 (15). Following DSBs, the Ku complex recognizes the ends of DSBs and activates DNA-PKcs and its dependent signal transduction pathway (16–19), which facilitates non-homologous end joining (NHEJ) repair for DSBs (20,21). Although the Ku70/80 complex is an abundant protein complex (22), once it is loaded on the DNA strand, it does not directly cap the broken end of DSBs. Instead, both Ku70 and Ku80 make several contacts with the DNA backbone of the double-strand helix (15,17).

PARP1, the founding member of PARP family enzymes, is known to be a sensor of DNA single-strand breaks (SSBs)

*To whom correspondence should be addressed. Tel: +1 626 218 5724; Email: xyu@coh.org

(23,24). PARP1 contains multiple domains including three N-terminal Zinc Finger motifs (ZF1-ZF3), a BRCT domain, a WGR domain and a C-terminal catalytic domain (25). Once an SSB is generated, ZF1 and ZF2 motifs coordinately and quickly capture the 5′- and the 3′-ends of the SSB, which in turn repositions the ZF3 and the WGR domains by creating additional intramolecular contact sites, releases the helical motif inside the catalytic domain, and exposes the NAD^+ binding site for PARylation (26). PARP1 is also one of the most abundant nuclear polypeptides in the nucleus (27). On average, one PARP1 molecule is able to cover ∼10 nucleosomes on the chromatin (28). Thus, the huge abundance of PARP1 allows rapid detection of SSBs (29), which is the most frequent form of DNA lesion within the cells.

Aside from SSBs, structural analysis of PARP1 suggests that it can recognize DSBs as well (30). DSBs are the most deleterious type of DNA lesions, and PARP1 adopts slightly different recognition modules to recognize DSBs. One DSB generates two ends on the DNA double-strand helix, and the ZF1 motif of PARP1 is able to recognize the terminal base pair at one end. At the same end, ZF3 along with the WGR domain reside in the minor and the major grooves, respectively, to contact each side of the backbone of DNA helix and stabilize the interaction; in addition, the WGR domain stacks against the riboses at the 5′-terminus of the DNA. In contrast, ZF2 is dispensable for DSB recognition. The intricate interaction with one end of DSB triggers intramolecular conformational changes that unfolds helical subdomain of the catalytic domain. The helical subdomain acts as an autoinhibitory domain and its unfolding relieves the inhibitory effect of NAD^+ binding (30). Thus, PARP1 could also be an important sensor for DSBs. Once PARP1 recognizes DNA ends, it quickly catalyzes PARylation at the DNA damage sites, which in turn mediates the early recruitment of numerous DNA damage repair factors to repair the lesions (24,31–33).

Recent studies have reported that sirtuins are also able to relocate to DNA lesions quickly, and might even play a role in activating PARP1 (34–36). Cells deficient in Sirt1 or Sirt6 have defective DSB response, indicating that sirtuins may be involved in DSB sensing (37,38). However, as sirtuins are deacetylases, it is unclear if chromatin deacetylation triggers any signal cascade for DNA damage repair.

Here, we systematically examined the recruitment kinetics of DSB sensors, and found that PARP1 and the Ku complex reached the DNA lesions much earlier than other possible sensors. Using a super-resolution fluorescence imaging system, we further studied the recruitment profile of PARP1 and the Ku complex, and observed that these two DSB sensors recognized DSBs in different cell cycle phases. Moreover, PARP1 was able to remove the Ku complex from the DSBs through its enzymatic activity.

MATERIALS AND METHODS

Cell culture

The cell line NIH-3T3 containing LacO and I-SceI recognition site was a gift from Dr. Sethuamasundaram Pitchiaya (University of Michigan) (39). The cells were cultured in DMEM supplemented with heat-inactivated fetal calf serum, penicillin (100 U/ml), and streptomycin (100 μg/ml) in a tissue culture incubator with 5% CO_2 at 37°C.

Plasmids and transfection

To construct the vector expressing blue fluorescent protein (BFP) tagged-LacI, a BFP coding sequence was amplified from a backbone expressing BFP (Plasmid #45564, Addgene) and LacI was amplified from the pGEX-4T1 vector. BFP and LacI were then subcloned into pCDNA3.1(+) vector. The transfection of plasmid was performed using Lipofectamine 2000 (Invitrogen) according to the manufacturer's instructions.

Protein purification and labeling

His-PARP1, the His-PARP1 E988K mutant, and the GST-Ku70/80 complex were purified from SF9 insect cells. SF9 cells were infected with correlated baculoviruses for 48 h, then cells were collected, washed with PBS and lysed with ice-cold NETN100 buffer. The soluble fraction was incubated with glutathione-sepharose beads and eluted with glutathione. After dialyzed into a phosphate buffered saline at pH 7.4, the proteins of PARP1 and Ku70/80 were then purified by fast protein liquid chromatography and concentrated by a centrifugal filter unit (Millipore). For protein labeling, PARP1 and Ku70/80 proteins were further prepared and labeled with Alexa Fluor 647 and Alexa Fluor 532 respectively, according to the instruction of the protein labeling kit (Life Sciences).

Microinjection and intracellular single-molecule imaging

NIH-3T3 cells (1×10^5) were seeded onto delta-T dishes (Bioptechs) and transfected with the vector expressing BFP-LacI one day before microinjection. The regular DMEM was replaced with phenol red-free medium 4 h prior to microinjection. Immediately before microinjection, the cell culture medium was replaced with a minimal HEPES buffered saline (HBS) medium without serum and vitamins, but containing 20 mM HEPES–KOH (pH 7.4), 135 mM NaCl, 5 mM KCl, 1 mM $MgCl_2$, 1.8 mM $CaCl_2$ and 5.6 mM glucose. The micropipette (Femtotip, Eppendorf) was loaded with ∼0.5 amol fluorophore-labeled proteins. Twenty fg of I-SceI and Trex2 were also added to the microinjection system. Live cells with a BFP dot were selected for imaging. We used HILO illumination to image cells at 120× magnification with 30 ms camera exposure on two Andor iXon Ultra EMCCD cameras using a cell-TIRF system on an Olympus IX81 microscope.

In vitro imaging assay

Coverslips were boiled and washed with hydrochloric acid. Then they were put in the poly-lysine solution (Sigma) for 1 h at room temperature, and washed twice with water. Plasmids were sequentially diluted with water and incubated with the prepared coverslips for another 1 h at room temperature, and then the coverslips were washed twice in water. Coverslips were further stained with DAPI for 30 min at room temperature, followed by two washes with water.

Coverslips with proper density of DAPI signal were selected for *in vitro* imaging. DAPI staining was used to localize the DNA molecules, then the solution containing 0.1 nM PARP1, the Ku complex, and/or 10 μM NAD^+ was added to the area of interest.

In vitro PARylation assay or Ku70 PARylation assay in U2OS cell

One μg recombinant GST-Ku70/80 protein was incubated with or without 3 μg His-PARP1 or the E988A mutant at room temperature for 1 h, in the presence of NAD^+ and DNA oligo activator. Then, the beads were thoroughly washed in ice-cold PBS three times and then boiled in the SDS sample buffer for further analysis. To detect the PARylated Ku complex, U2OS cells were treated with MMS for 30 min and then lysed with NETN100 buffer. The cell lysate was incubated with Ku70 antibody overnight. Then the immunoprecipitated Ku complex was examined by western blotting.

Data analysis

Single particles were tracked using Imaris (Bitplane). For colocalization assay, particles were firstly tracked using Imaris, and then in-house MATLAB routines were used to detect the potential colocalized particles from different channels. These particles were further manually confirmed. The plots displaying the fluorescence intensity were generated with ImageJ.

Cell cycle synchronization

The NIH-3T3 cells were synchronized at the G1/S boundary by double thymidine block. The cells were incubated with 2 mM thymidine for 14 h, washed extensively with PBS and released for 8 h followed by a second thymidine block for 14 h and released.

MTT assay

The NIH-3T3 cells were seeded in 96-well plates at a density of 5000 cells in 150 μl medium per well. After cells were synchronized by double thymidine block, 1 μM olaparib was added to the cells in triplicate. The plates were incubated at 37°C in 5% CO_2 for 2 h and then subjected to 5 Gy of ionizing radiation (IR). Cells were then incubated at 37°C for 48 h. Twenty μl MTT solution (5 mg/ml, dissolved in PBS) was added to each well, and the plates were incubated at 37°C for additional 4 h. Then the supernatant was discarded, and 200 μl DMSO was added to dissolve the formazan product. The absorbance at 570 nm (A570) was determined with a multi-well plate reader.

Immunofluorescence staining

Cells were synchronized by double thymidine block and then subjected to 2 Gy of IR. After recovery for 3 h, cells were washed with PBS, and fixed with 4% paraformaldehyde for 20 min at room temperature. Then cells were permeabilized with 0.5% Triton X-100 for 10 min at room temperature and washed again with PBS. After blocking with 8% goat serum, cells were incubated with primary antibodies at 4°C overnight, washed with PBS three times, incubated with the secondary antibody for additional 1 h at room temperature, and washed with PBS three times before imaging. Foci number in each nucleus was calculated with ImageJ and the maximum foci number per cell was counted as 100% in each experiment.

Repair assays

EJ5-GFP, EJ2-GFP and GR-GFP reporters that were used to analyze c-NHEJ, alt-NHEJ and homologous recombination (HR) pathways were the generous gifts from Dr. Jeremy Stark (Beckman research institute, City of hope) (40). Cell lines were infected with the virus encoding I-SceI-GR for three days, and then the cells were synchronized with double thymidine block. The translocation of I-SceI-GR into the nucleus was induced by treatment of 0.1 mM triamcinolone acetonide (TA). The rate of GFP positive cells were examined by FACS.

RESULTS

Both PARP1 and the Ku complex quickly and independently relocate to DNA lesions

To study the time-dependent relocation of DSBs sensors, we examined the recruitment kinetics of the MRN complex, the RPA complex, the Ku complex, PARP1 and sirtuins to the sites of DNA damage induced by laser microirradiation. We labeled NBS1, RPA2, Ku70, Ku80, PARP1, and SIRT6 with GFP tag to track their relocations with live cell imaging. Notably, both PARP1 and the Ku complex reached the DNA lesions in around 1 s post-damage (Figure 1A). In contrast, the MRN complex and SIRT6 were recruited after 10 s following DNA damage. The RPA complex accumulated at the DNA lesions in around 30 s following laser microirradiation (Figure 1A). The different recruitment kinetics suggests that these factors may play different roles in DNA damage repair process. Since both PARP1 and the Ku complex are highly expressed in cells, and respond quickly upon DNA damage, we reasoned that PARP1 and the Ku complex recognize DNA lesions earlier than other DNA damage response factors. Thus, we selected PARP1 and the Ku complex for further analysis and tried to elucidate if the recruitment of PARP1 and the Ku complex is dependent on each other.

To study the potential functional interaction between PARP1 and the Ku complex during the DNA damage response, we examined the recruitment of PARP1 in the *Ku70*$^{-/-}$ MEFs and that of Ku70 in the *Parp1*$^{-/-}$ MEFs. However, the recruitment kinetics of PARP1 or Ku70 was unaffected comparing to those in the wild-type MEFs (Figure 1B and C), suggesting that the recruitment of PARP1 and the Ku complex are independent of each other.

Live cell super-resolution imaging measures the recruitment kinetics of PARP1 and the Ku complex

Although laser microirradiation allows us to roughly calculate the recruitment kinetics, it generates a mixture of complicated DNA lesions due to the non-specific nature of UV

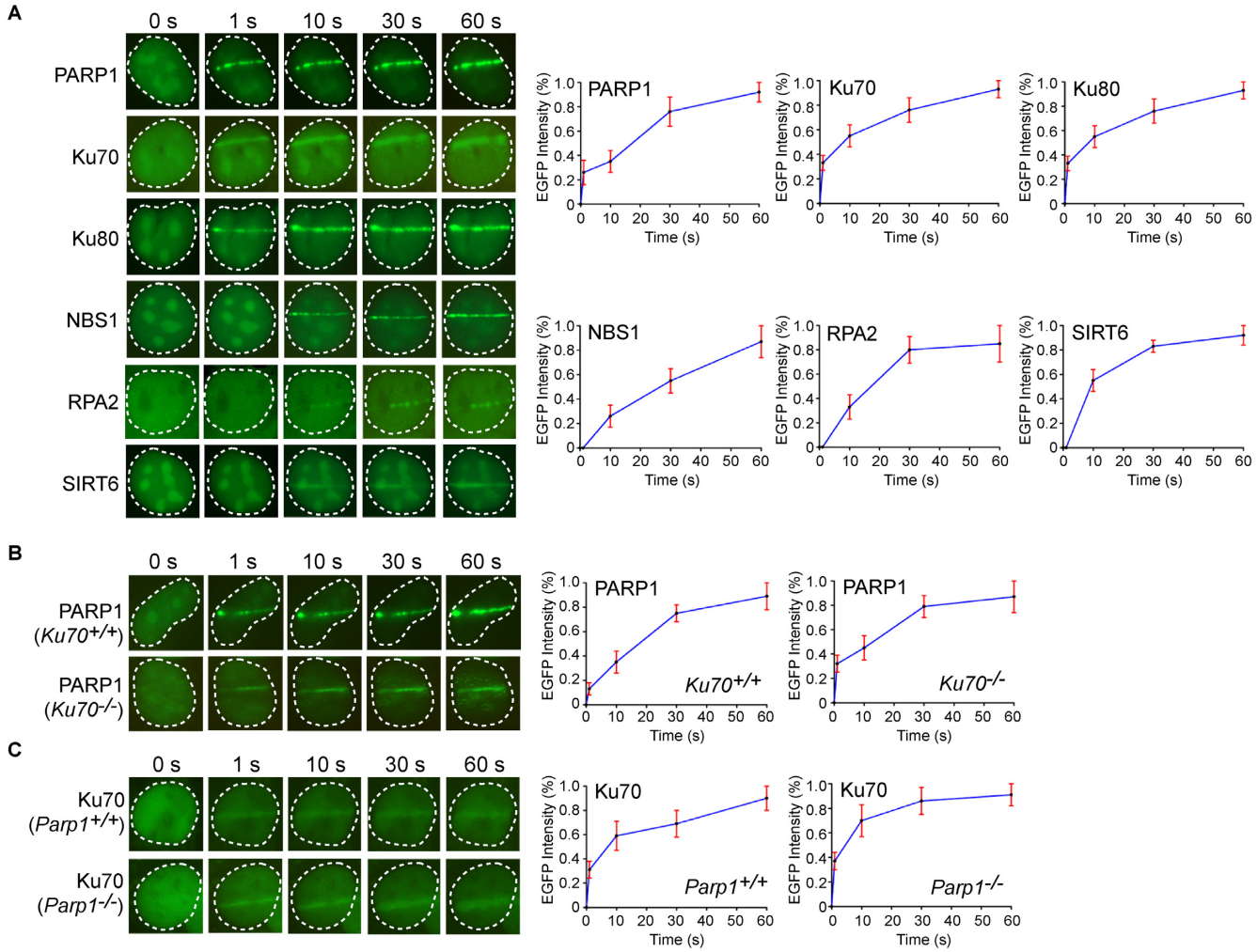

Figure 1. Recruitment kinetics of potential DNA damage sensors. (**A**) The relocation kinetics of PARP1, Ku70, Ku80, NBS1, RPA2, and SIRT6 to the DNA damage sites. GFP-tagged proteins were expressed in U2OS cells, and the relocation kinetics was monitored at different time points following laser microirradiation. (**B**) The relocation kinetics of PARP1 to the DNA damage sites. GFP-PARP1 was expressed in wild-type ($Ku70^{+/+}$) or $Ku70^{-/-}$ MEFs. (**C**) The relocation kinetics of Ku70 to the DNA damage sites. The GFP-Ku70 was expressed in wild-type ($Parp1^{+/+}$) or $Parp1^{-/-}$ MEFs. The GFP signal intensity at the microirradiation area was measured with ImageJ and represented in the right.

irradiation. Moreover, it is difficult to accurately measure the kinetics, especially for the early recruited DNA damage sensors. Thus, we established a super-resolution fluorescence imaging system to monitor the recruitment of PARP1 and the Ku70/80 complex in more detail.

In this system, we firstly constructed a vector with a BFP tag at the 5′ of LacI cDNA and expressed the BFP-LacI fusion protein in the NIH/3T3 cell containing the LacO sites as well as a single I-SceI site. As the BFP-LacI protein recognizes the LacO site, the localization of the unique I-SceI site in the nucleus is able to be determined by monitoring the blue fluorescence with highly inclined and laminated optical sheet (HILO) microscopy (Figure 2A). The recombinant I-SceI protein was microinjected into the nucleus along with the recombinant PARP1 or the Ku70/80 complex proteins. Based on the kinetics of I-SceI, the median time of cleavage at the I-SceI site in each injected cell is expected to be within the millisecond range (41). When we determined the relocation kinetics of PARP1, we found that its average relocation time to the DSB was 812 ms (Figure 2B), which is in a similar range as observed with laser microirradiation. We similarly examined the Ku complex and found that it reached the site of DNA damage with an average time of 737 ms (Figure 2C), which is slightly faster than PARP1, but not statistically significant (Figure 2D). Thus, our data suggest that PARP1 and the Ku complex are recruited to the DSB almost at the same time.

When we compared the average dwelling time for PARP1 and Ku complex at the break site, we observed that neither PARP1 nor the Ku complex stayed at the DSB for a prolonged time. The average dwell time of PARP1 at the DSB is 902 ms, whereas that of the Ku complex is 938 ms, only insignificantly longer (Figure 2E). It is possible that other secondary DNA damage sensors or DSB repair machinery have been loaded onto the DSB by this time, which in turn replaced the primary sensors, such as PARP1 and the Ku complex, for damage-induced signal transduction or lesion repair. Alternatively, the recognition of the DSB by these

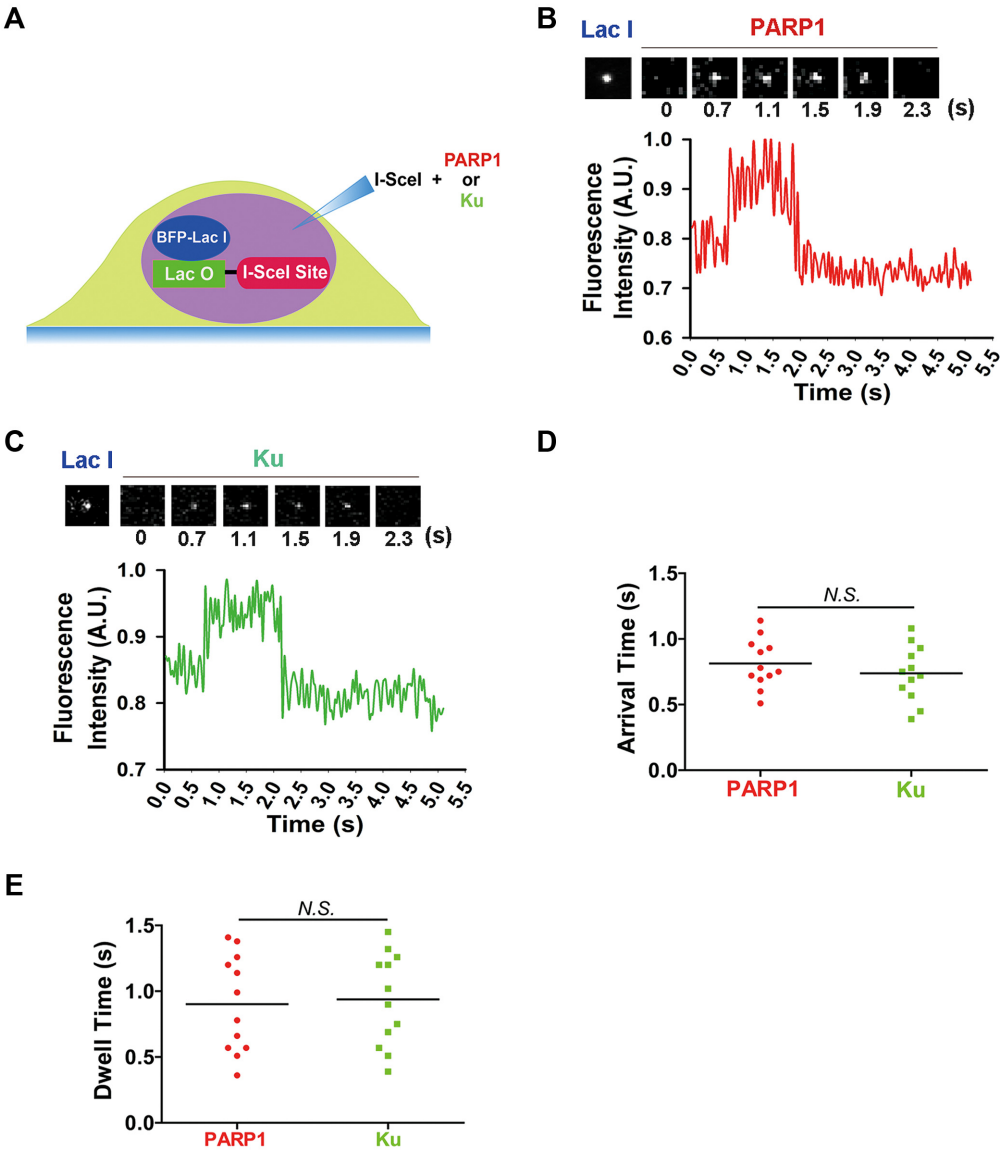

Figure 2. Single molecule imaging reveals the recruitment kinetics of PARP1 and the Ku complex in live cells. (**A**) The experimental system for investigating the recruitment of a single PARP1 or Ku complex molecule to the DSB in live cells. (**B**) The recruitment kinetics of PARP1 at the DSB. Plots represent PARP1 fluorescence intensity recorded at the DNA damage site. BFP-LacI indicates the DSB site. Insets show fluorescence images taken at the indicated time points. (**C**) The recruitment kinetics of a single Ku complex to the DSB. (**D**) Distribution of the arrival time of PARP1 (n = 12) or the Ku complex (n = 12) at the DSB. (**E**) Distribution of the dwell time of PARP1 or the Ku complex at the DSB. Mann-Whitney U test was performed to analyze the group difference. A. U., arbitrary unit; N. S., nonsignificant ($P > 0.05$).

sensors works as an on-off cycle. The labeled PARP1 and the Ku complex were replaced by the endogenous unlabeled sensors.

PARP1 and the Ku complex compete with each other to relocate to the DSBs

Since PARP1 and the Ku complex reach the DSB at almost the same time, we examined the functional interactions between these two damage sensors. We simultaneously microinjected PARP1 and the Ku complex labeled with different fluorescence molecules into the nucleus, and measured the kinetics. We found that the DSB was occupied by either PARP1 or the Ku complex (Figure 3A). We did not observe both molecules co-localizing at a single DSB, indicating that PARP1 and the Ku complex may compete with each other to occupy a DSB end. Moreover, both the arrival time and the dwell time of PARP1 and the Ku complex in the co-injection assay are similar to those in the single injection assay (Figure 3A).

However, the majority of the cells were occupied by the Ku complex when cells were injected with PARP1 and the Ku complex mixture (Figure 3B). Notably, we found that the ratio of the Ku complex-occupied DSBs to the PARP1-occupied DSBs in unsynchronized cells is close to the ratio of G1 to S phase cells. Thus, we examined the role of cell cycle in regulating these events. When we synchronized cells at the G1/S boundary with the double thymidine block,

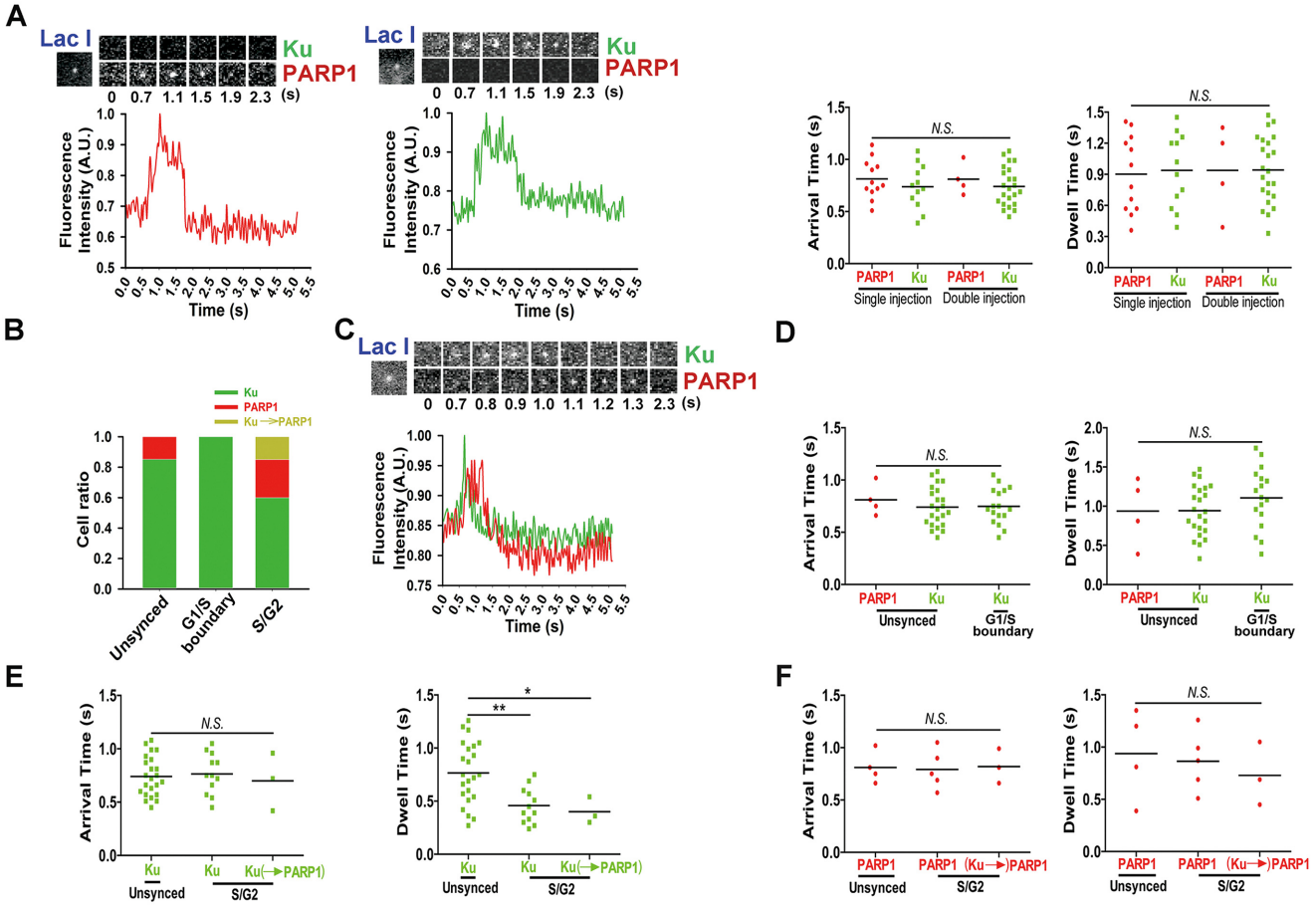

Figure 3. PARP1 and the Ku complex compete with each other to occupy the DSB. (**A**) PARP1 and the Ku complex compete with each other to relocate to the DSB. Single PARP1 or Ku complex was examined at the DSB. Mann–Whitney U test was performed for analyzing the difference in the arrival time or dwell time between PARP1 and the Ku complex at the DSB. N.S.: nonsignificant ($P > 0.05$). (**B**) The ratio of PARP1 and the Ku complex at the DSB. Ku→PARP1 represents an event in which the Ku complex is the first to reach the DSB and subsequently gets replaced by PARP1. Cells were synchronized and released at the G1/S boundary or S/G2 phase by double thymidine block.(**C**) The representative event shows that PARP1 can remove the Ku complex at the DSB in S/G2 cell. (**D**) Analysis of the difference in the arrival time and the dwell time of PARP1 or the Ku complex between unsynchronized cells and cells at the G1/S boundary. (**E**) Analyzing the difference in the arrival time ($P > 0.05$) and the dwell time ($P < 0.01$) of Ku complex between unsynchronized cells and S/G2 cells. (**F**) Analysis of the difference of the arrival time and the dwell time of PARP1 between unsynchronized cells and S/G2 cells. Statistical significance in D–F was tested using Mann–Whitney U test, N.S.: nonsignificant ($P > 0.05$).

we found that the DSB was occupied by the Ku complex. In contrast, when cells were released from the thymidine block and were in the S/G2 phase, the PARP1-occupied DSB events were significantly increased (Figure 3C). These results suggest that PARP1 and the Ku complex may sense the DSB in different cell cycle stages.

Notably, we found that when the Ku complex inhabited the DSB in the S/G2 cells, PARP1 was able to reach the DSB immediately after the Ku complex and appeared to replace the Ku complex at the damage site (Figure 3B and C). In contrast, we did not find that the Ku complex replaced PARP1. Collectively, these results indicate that PARP1 may be able to actively remove the Ku complex from the DSB in the S/G2 phase if the DSB was occupied by the Ku complex, but not vice versa.

We also examined the arrival and dwell time of PARP1 and the Ku complex in G1 or S/G2 cells. At the G1/S boundary, the DSB was entirely occupied by the Ku complex while PARP1 was completely absent at the damage site. The arrival time of the Ku complex in the G1 cells is very similar to that of the Ku complex in the unsynchronized cells. Although the dwell time of the Ku complex at the G1/S boundary is slightly longer than that in the unsynchronized cells, we did not observe a significant difference (Figure 3D). However, in the S/G2 cells, the dwell time of the Ku complex is significantly shorter than that in the unsynchronized cells, whereas the arrival time remains unchanged (Figure 3E). As the dwell time of the Ku complex is similar to those specific events that the Ku complex was replaced by PARP1 at DNA lesions (Figure 3C). We, therefore, posit that the injected Ku complex is likely removed by endogenous PARP1; that is, even though the Ku complex can occupy the DSB in the S/G2 cells, our data are consistent with the notion that it is then rapidly replaced by PARP1. In contrast, both the arrival and the dwell time of PARP1 remains unchanged in the S/G2 cells (Figure 3F). Collectively, these results suggest that the Ku complex

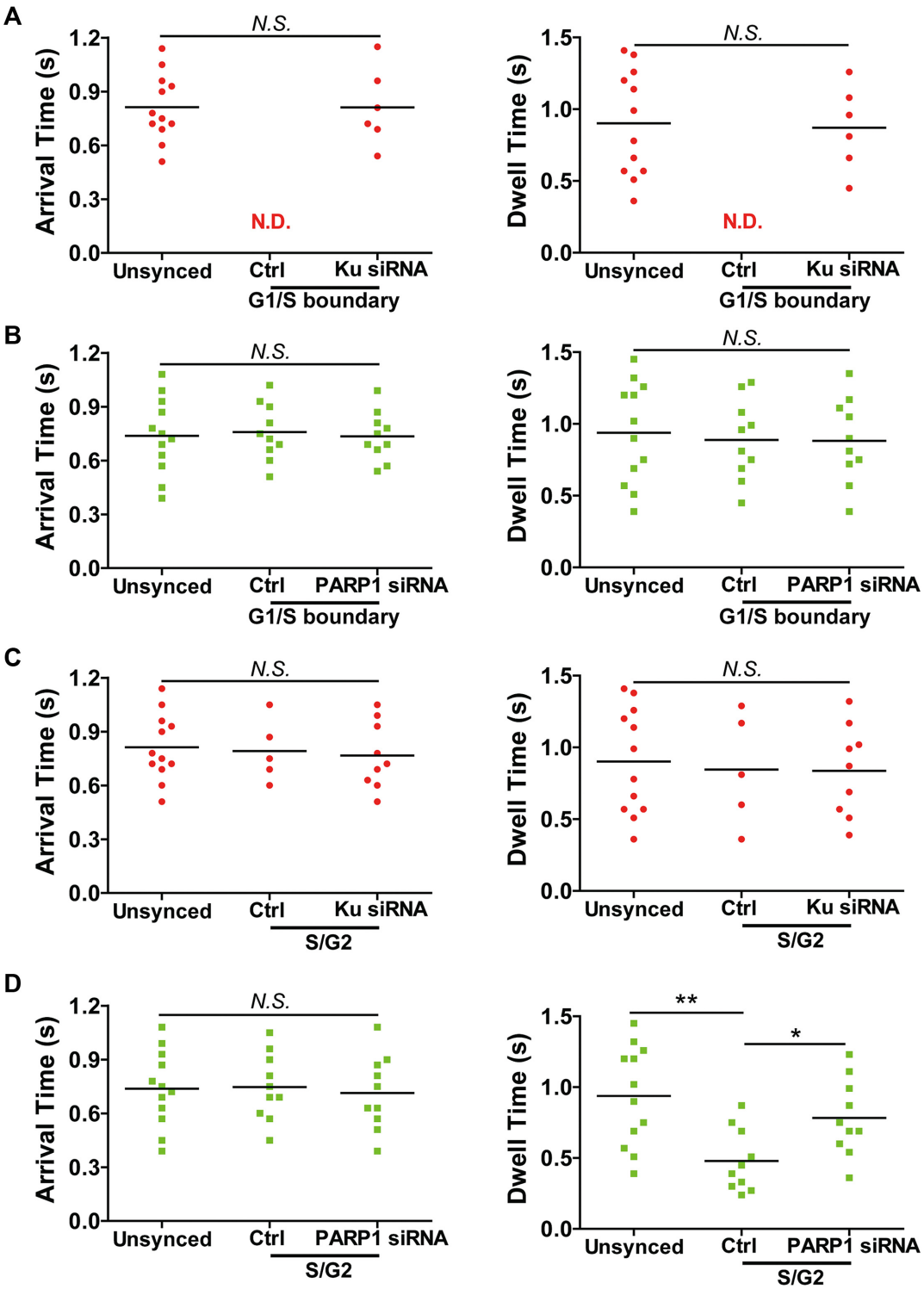

Figure 4. Lacking endogenous PARP1 or the Ku complex regulates each other for the DSB relocation. (**A**) Lacking the Ku complex does not promote PARP1 occupancy at the DSB in the G1/S phase. The arrival and the dwell time of PARP1in the cells at the G1/S boundary were compared to those in the unsynchronized cells. (**B**) Lacking PARP1 does not affect the relocation of the Ku complex in the G1 cells. (**C**) The PARP1 relocation in the S/G2 cells is unaffected in the absence of the Ku complex. (**D**) Lacking PARP1 prolongs the retention of the Ku complex at the DSB in the S/G2 cells. The arrival time and the dwell time of the Ku complex in the S/G2 phase were compared to those in the unsynchronized cells. *, $P < 0.05$; ** $P < 0.01$; N.S.: nonsignificant ($P > 0.05$).

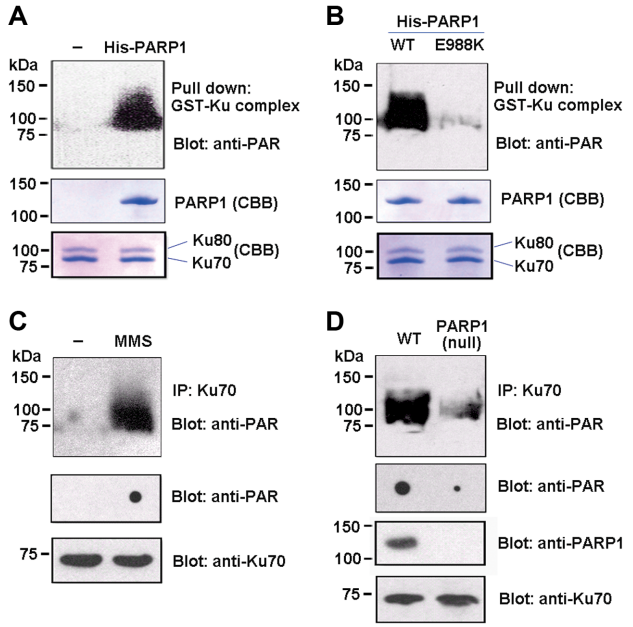

Figure 5. PARP1 PARylates the Ku complex. (**A**) PARP1 PARylates the Ku complex *in vitro*. The recombinant proteins were examined by SDS-PAGE and Western blotting with indicated antibodies. The loaded proteins were also examined by Coomassie blue staining. (**B**) The enzymatic activity of PARP1 is required for the PARylation of the Ku complex. The E998A mutant was examined in the *in vitro* PARylation of the Ku complex. (**C**) The Ku70 is PARylated in response to DNA damage. U2OS cells were treated with 5 μM MMS for 30 min. The Ku complex was examined by indicated antibodies. The level of PARylation in the whole cell lysates was examined by the anti-PAR antibody. (**D**) PARP1 is required for the PARylation of the Ku complex. Both U2OS cells and PARP-null cells were treated with MMS. The PARylation level of the Ku complex was examined.

senses the DSB in the G1 cells, whereas PARP1 is likely to play an important role in sensing the DSB in the S/G2 cells.

PARP1 competes with the Ku complex to occupy the DSB in the S/G2 cells

To study the functional interaction between PARP1 and the Ku complex, we knockdown the endogenous PARP1 or the Ku complex with siRNAs, and then observed the relocation of ectopic PARP1 and the Ku complex. At the G1/S boundary, when the endogenous Ku complex was depleted (Supplementary Figure S1), PARP1 was able to relocate to the DSB, in stark contrast to the lack of PARP1 recruitment to the DSB when the endogenous Ku complex is abundant. The arrival and the dwell time of PARP1 were similar to those in the unsynchronized cells (Figure 4A). However, at the G1/S boundary, knockdown of PARP1 did not affect the arrival or dwell time of the Ku complex (Figure 4B). Thus, these results indicate that the Ku complex competes out PARP1 in the G1 cells, but not vice versa.

In contrast, loss of the Ku complex did not affect the relocation kinetics of PARP1 in the S/G2 cells (Figure 4C). However, lacking endogenous PARP1 significantly prolonged the dwell time of the Ku complex (Figure 4D). These finds suggest that PARP1 is able to displace the Ku complex from a DSB in the S/G2 cells. Taken together, our data indicate that the Ku complex is likely to play a predominant role in sensing the DSB in the G1 cells, whereas PARP1 is able to recognize and replace the Ku complex in the S/G2 cells.

The Ku complex is a substrate of PARP1

Since PARP1 is able to replace the Ku complex at the DSB in the S/G2 cells, we next asked if the Ku complex is a substrate of PARP1. We first performed an *in vitro* PARylation assay by incubating the Ku complex with PARP1. We found that the Ku complex was conjugated with poly(ADP-ribose), suggesting that PARP1 catalyzes PARylation on the Ku complex (Figure 5A). Compared with the wild-type PARP1, the E988A mutant that loses its catalytic activity failed to PARylate the Ku complex (Figure 5B).

Next, we treated U2OS cells with methyl methanesulfonate (MMS) to induce DNA damage, immunoprecipitated the Ku complex from the cell lysates, and detected the PARylation of the Ku complex (Figure 5C). In contrast, lacking PARP1, the PARylation of the Ku complex was remarkably impaired (Figure 5D). Collectively, these results suggest that the Ku complex is PARylated by PARP1 in response to DNA damage.

PARylation of the Ku complex facilitates its removal from the DSBs

To test if the PARylation of the Ku complex is important for the removal of the Ku complex from DSBs, we established an *in vitro* DNA end recognition assay. We immobilized pCDNA3 plasmids on glass slides coated with poly-lysine. Since both PARP1 and the Ku complex cannot recognize the circular plasmid DNA, we digested it with EcoRV to create DSBs with blunt ends. The recombinant PARP1 and the Ku complex were added to flow through the DNA conjugated slides. In the absence of NAD^+ (ADP-ribose donor in PARylation), DSBs were recognized by either PARP1 or the Ku complex (Figure 6A), and both of them stayed at DSBs for a prolonged time (Figure 6B). Strikingly, upon NAD^+ was added to activate the enzymatic activity of PARP1, we found that a subset of the Ku complex was replaced by PARP1 at DSBs. Not only the dwell time of PARP1 was remarkably reduced, but also the Ku complex was removed by PARP1 in a very short period of time (Figure 6C). Within the 5 seconds of observation time, we even found two rounds of on and off cycle of PARP1 (Figure 6C). We also observed a subset of the Ku complexes still localized at DSBs for a prolonged time owing to a low nM concentration of PARP1 used in this *in vitro* assay (Figure 6D). And not all the Ku complex is able to be PARylated in this short observation time (5 s). Moreover, we compared wild type PARP1 and the E988A mutant for their ability to remove the Ku complex, and found that although E988A mutant occupied the DSBs, it cannot remove the Ku complex (Figure 6D). When both the Ku complex and the E988A mutant were incubated with DSBs, none of these proteins were dissociated from the DSBs. Thus, these results suggest that the enzymatic activity of PARP1 plays a key role in removing the Ku complex and PARP1 itself from the DSBs (Figure 6E).

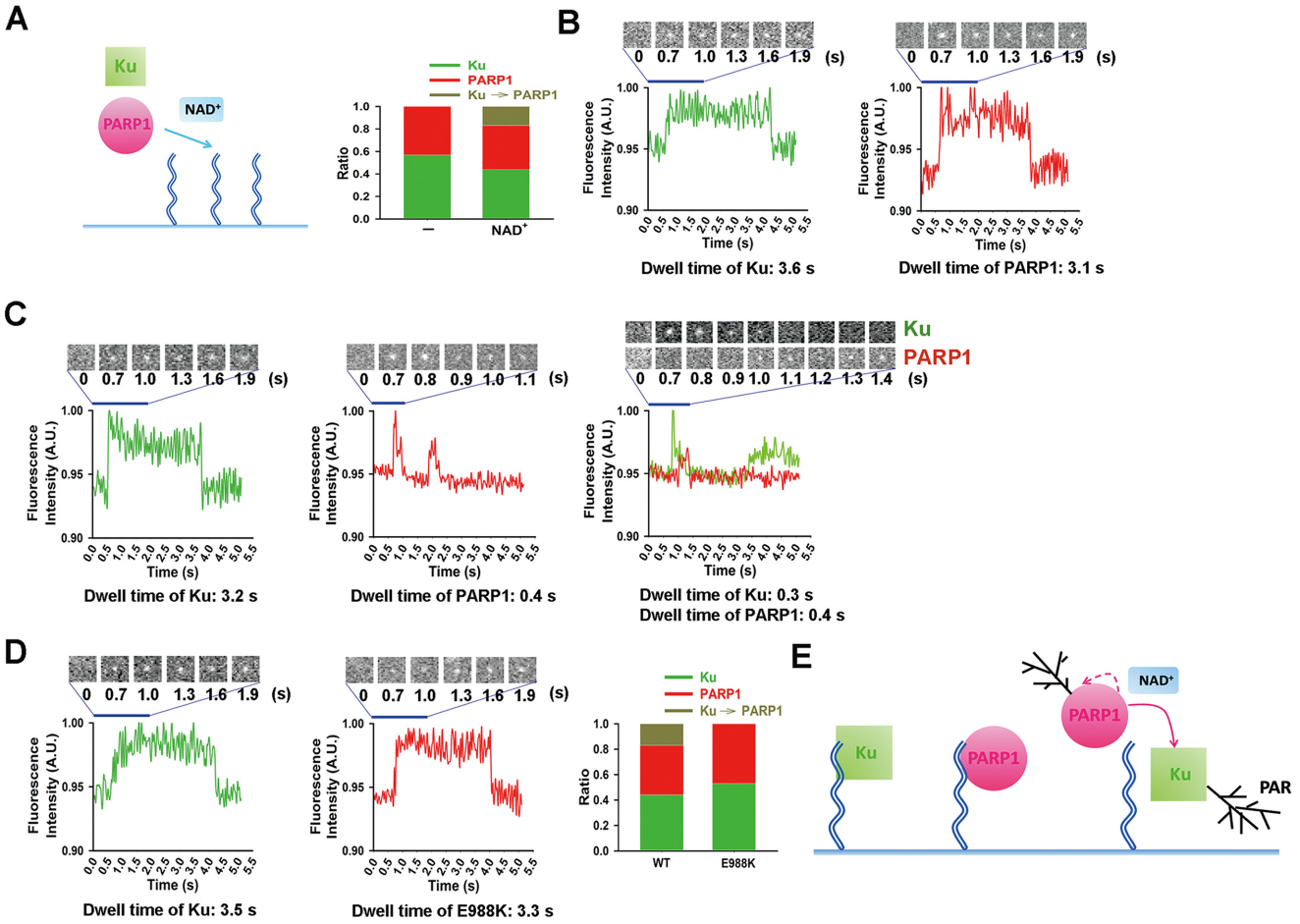

Figure 6. PARP1 replaces the Ku complex in the presence of NAD^+. (**A**) A schematic model describing the *in vitro* competition assay between PARP1 and the Ku complex to occupy the DSBs. The histogram shows the ratio of the DSBs occupied by PARP1, the Ku complex or Ku complex replaced by PARP1 (Ku→PARP1). (**B**) In the absence of NAD^+, PARP1 and the Ku complex occupy the DSBs for a prolonged time. Representative plots display PARP1 or the Ku complex at the DSBs. Dwell time of PARP1 and the Ku complex were measured. (**C**) In the presence of NAD^+, PARP1 is able to remove the Ku complex from the DSBs. Three representative plots are shown. (**D**) The E988A mutant of PARP1 cannot remove the Ku complex. Representative plots were included. (**E**) A schematic model depicting PARP1-dependent removal of the Ku complex.

PARP1 is involved in alt-NHEJ in the S/G2 phase

As PARP1 is able to release the Ku complex in the S/G2 phase, we further examined the physiological function of PARP1 in the DSB repair in the S/G2 phase. It has been shown that PARP1 regulates alternative NHEJ (alt-NHEJ), whereas the Ku complex mediates the canonical NHEJ (c-NHEJ) (2). The major difference between these two DSB repair pathway is that the DSB ends need to be further processed into single-strand DNA (ssDNA) overhang in the first step of alt-NHEJ. As the RPA complex coats the ssDNA overhang, we used phosphor-Rpa2 as the surrogate marker to examine the DSB end resection. In agreement with previous study (2), inhibition of PARPs activity suppressed the foci formation of phosphor-Rpa2 when cells were in the S/G2 phase (Figure 7A). Consistently, inhibition of PARPs activity impaired the alt-NHEJ when cells are in the S/G2 phase (Figure 7B and Supplementary Figure S2). And we observed a modest reduction of cell viability when the S/G2 cells were treated with IR (Figure 7C). Taken together, these results suggest that PARP1 plays an important role in the alt-NHEJ pathway for DSB repair in the S/G2 phase.

DISCUSSION

Compared with other DNA lesions, DSBs are not only the most deleterious type of lesions, but also the rarest lesions (42). In this study, we have shown that among the six DSB sensors, PARP1 and the Ku complex are recruited to the sites of DNA damage much earlier than others. The results are correlated with the fact that the endogenous steady-state expression levels of these two DSB sensors are the highest among all the sensors, consistent with the expectation that a bimolecular damage sensing process of a rare lesion will be faster at higher sensor concentration. Thus, PARP1 and the Ku complex might be the primary sensors for DSBs. Rapid detection will be very critical for a swift repair and maintaining genomic stability.

With laser microirradiation, both PARP1 and the Ku complex get to the sites of DNA damage within one second. Due to technical limitations, laser microirradiation is

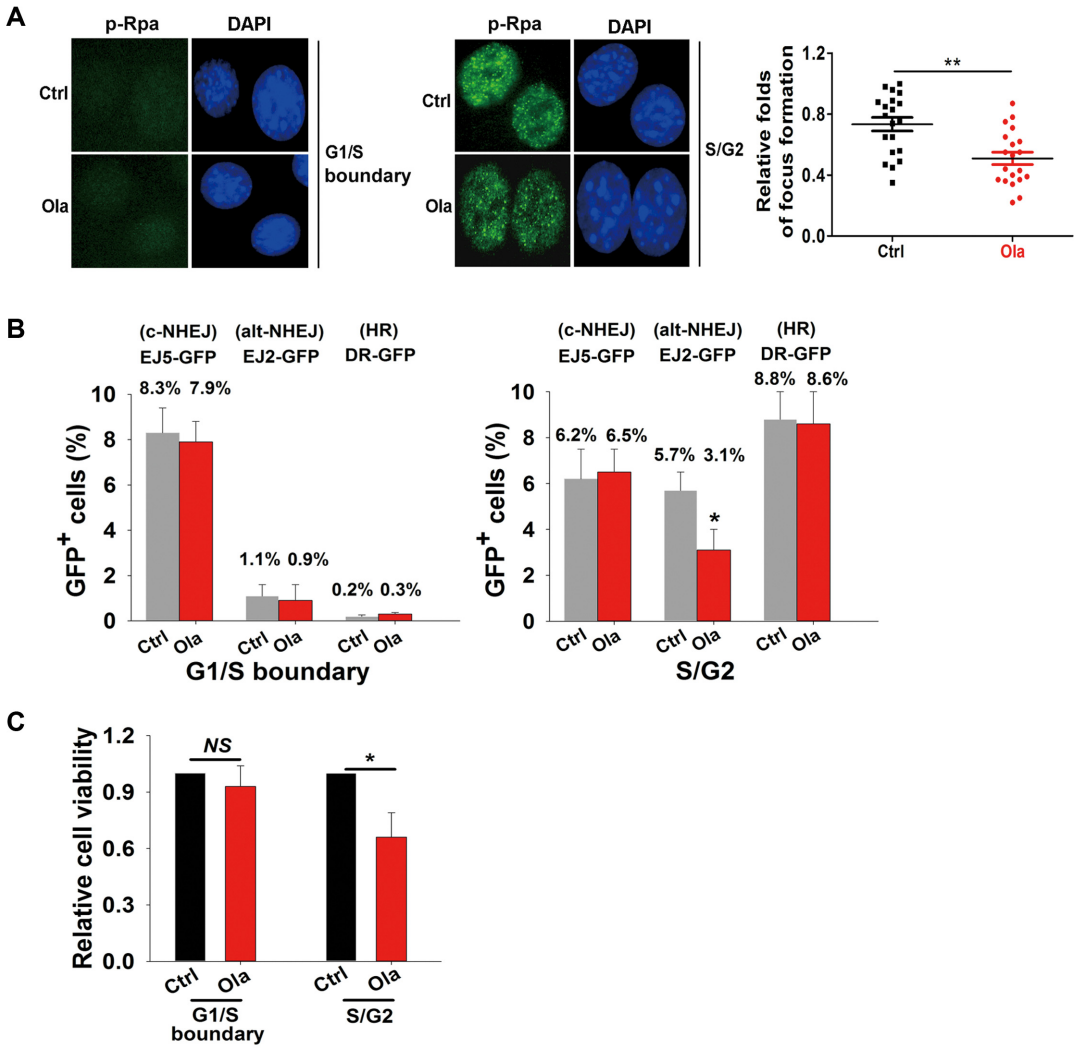

Figure 7. PARP1 plays an important role in DSB repair. (**A**) PARP1 is involved in DSB end processing. The NIH-3T3 cells at G1/S boundary or in the S/G2 phase were treated with or without 1 μM olaparib (Ola) followed by 2 Gy of IR. The foci of phosphor-Rpa2 (p-Rpa) were examined at the G1/S boundary (left panel) or in the S/G2 phase (middle panel). The relative fold change of foci formation was summarized in the right panel (**$P < 0.01$). (**B**) PARP1 is involved in alt-NHEJ in S/G2 phase. Three independent experiments were performed. Data were presented as mean ± SD (*$P < 0.05$). GFP reporter assays were used to examine c-NHEJ, alt-NHEJ and HR. The GFP positive cells were measured. (**C**) PARP1 plays an important role in maintaining cell viability in response to IR. The NIH-3T3 cells at G1/S boundary or in the S/G2 phase were treated with or without 1 μM olaparib followed by 5 Gy of IR. The MTT assays were performed to measure the cell viability. Three independent experiments were performed. Data were presented as mean ± SD (*$P < 0.05$).

not able to reveal the details of the recruitment kinetics. Thus, we established an assay in live cells to examine the kinetics of PARP1 and the Ku complex recruiting to a single DSB, induced by a site-specific restriction enzyme I-SceI in the NIH/3T3 cells. Consistent with previous genetic studies (43–45), we found that PARP1 and the Ku complex compete with each other to recognize the DSB. Although both PARP1 and the Ku complex recognize DSB ends, PARP1 directly caps the ends, whereas the Ku complex slides onto the DNA double-strand helix without capping the ends (15). Based on the previous structural analysis, PARP1 and the Ku complex may be expected to coexist at DNA ends. However, we did not observe this event. Instead, once PARP1 is loaded to the DSB, it will remove the Ku complex via PARylation, indicating that PARP1 and the Ku complex compete with each other for the DSB repair.

Moreover, the loading of PARP1 and the Ku complex were distinct in different cell cycle phase (46,47). Specifically, in the G1 cells, we found that the DSB was occupied by the Ku complex, which was not replaced by PARP1. However, in the S/G2 cells, PARP1 occupied the DSB. It is possible that PARP1 and the Ku complex mediate distinct repair mechanisms in different cell cycle phases. It has been reported that the Ku complex initiates the c-NHEJ, whereas PARP1 regulates alt-NHEJ (2). Consistently, c-NHEJ is mainly accomplished in the G1 cells. Since alt-NHEJ need microhomology to mediate the DSB repair, it may preferentially happen in S phase (48). Thus, loading of different DSB sensors may determine the repair path-

way choice. Still, the factors that determine the loading of different sensors remain elusive. It is plausible that different chromatin status in different cell cycle phases may regulate the loading of different sensors. Alternatively, as the recruitment of these DNA damage sensors is very quick, it is possible that pre-deposited regulations such as alteration of post-translational modifications during cell cycle establish the condition for the recruitment of the Ku complex as well as PARP1.

Interestingly, we found that PARP1 is able to replace the Ku complex at DSBs in the S phase, which may facilitate the PARP1-dependent DSB repair. This replacement is dependent on the enzymatic activity of PARP1. Moreover, we found that after PARylation, the Ku complex dissociates from the DNA ends without the help of any chaperons, indicating that PARylation itself is sufficient to mediate the dissociation. In fact, auto-PARylation of PARP1 has been shown to mediate the PARP1 dissociation from the chromatin (49,50). Since PARylation installs substantial negative charges to the PARP1 substrates, the electrostatic repulsion between negatively charged PAR and DNA may assist the dissociation (51). Alternatively, ADP-ribose is a unique type of nucleic acid, and share some common features with deoxynucleic acid. Thus, the DNA-binding motifs of the Ku complex and PARP1 may become engaged by the PAR chains to facilitate the dissociation from the DSBs. Previous studies have demonstrated that PARylation serves as a signal to mediate the recruitment of DNA damage response factors to the sites of DNA damage (24,31). Here, we found that PARylation acts as a double-edged sword by facilitating the dissociation of these crucial proteins from DSBs. It is also possible that this post-translational modification regulates the sequential loading of DNA repair factors to coordinate the repair process. It is interesting to note that PARylation-mediated release of the Ku complex is earlier than that of PARP1 in the S/G2 phase. Thus, these events are likely sequential events at the DNA lesions. It may start from the PARylation of the Ku complex by PARP1. Once the Ku complex is released from the DNA, PARP1 has no other substrates but auto-PARylates itself, which releases PARP1 itself from lesions for the next step of the repair.

In addition to PARP1 and the Ku complex, other DSB sensors have been well studied (52). Although other DSB sensors are not recruited to the lesions as fast as PARP1 or the Ku complex, it is possible that these sensors may recognize DSBs with special features or under specific conditions. For example, the MRN complex may help recognize DSBs with 5′-overhangs, and is known to mediate HR in late S and G2 cells (53). Meanwhile, these sensors may have crosstalk during the DSB repair (24,31). In particular, some of the sensors can be PARylated or recognize PAR. Thus, while PARP1 and the Ku complex function as primary sensors, other factors may serve as secondary sensors. Multiple sensors may act together to trigger DSB repair.

SUPPLEMENTARY DATA

Supplementary Data are available at NAR Online.

ACKNOWLEDGEMENTS

We thank Drs. Sethuamasundaram Pitchiaya, Fabrizio D'Adda di Fagagna and Jeremy Stark for specific cell lines and reagents.

FUNDING

National Institutes of Health (NIH) [CA132755, CA130899, CA187209 to X.Y.]; NSF MRI-ID [DBI-0959823 to N.G.W.] for seeding the SMART Center. Funding for open access charge: NIH [CA130899].

Conflict of interest statement. None declared.

REFERENCES

1. Jackson,S.P. and Bartek,J. (2009) The DNA-damage response in human biology and disease. *Nature*, **461**, 1071–1078.
2. Ciccia,A. and Elledge,S.J. (2010) The DNA damage response: making it safe to play with knives. *Mol. Cell*, **40**, 179–204.
3. Blackford,A.N. and Jackson,S.P. (2017) ATM, ATR, and DNA-PK: The Trinity at the Heart of the DNA Damage Response. *Mol. Cell*, **66**, 801–817.
4. Stracker,T.H. and Petrini,J.H. (2011) The MRE11 complex: starting from the ends. *Nat. Rev. Mol. Cell Biol.*, **12**, 90–103.
5. Lee,J.H. and Paull,T.T. (2005) ATM activation by DNA double-strand breaks through the Mre11-Rad50-Nbs1 complex. *Science*, **308**, 551–554.
6. Paull,T.T. (2015) Mechanisms of ATM Activation. *Annu. Rev. Biochem.*, **84**, 711–738.
7. Savitsky,K., Bar-Shira,A., Gilad,S., Rotman,G., Ziv,Y., Vanagaite,L., Tagle,D.A., Smith,S., Uziel,T., Sfez,S. *et al.* (1995) A single ataxia telangiectasia gene with a product similar to PI-3 kinase. *Science*, **268**, 1749–1753.
8. Hopfner,K.P., Craig,L., Moncalian,G., Zinkel,R.A., Usui,T., Owen,B.A., Karcher,A., Henderson,B., Bodmer,J.L., McMurray,C.T. *et al.* (2002) The Rad50 zinc-hook is a structure joining Mre11 complexes in DNA recombination and repair. *Nature*, **418**, 562–566.
9. Paull,T.T. and Gellert,M. (1999) Nbs1 potentiates ATP-driven DNA unwinding and endonuclease cleavage by the Mre11/Rad50 complex. *Genes Dev.*, **13**, 1276–1288.
10. Shibata,A., Moiani,D., Arvai,A.S., Perry,J., Harding,S.M., Genois,M.M., Maity,R., van Rossum-Fikkert,S., Kertokalio,A., Romoli,F. *et al.* (2014) DNA double-strand break repair pathway choice is directed by distinct MRE11 nuclease activities. *Mol. Cell*, **53**, 7–18.
11. Williams,R.S., Dodson,G.E., Limbo,O., Yamada,Y., Williams,J.S., Guenther,G., Classen,S., Glover,J.N., Iwasaki,H., Russell,P. *et al.* (2009) Nbs1 flexibly tethers Ctp1 and Mre11-Rad50 to coordinate DNA double-strand break processing and repair. *Cell*, **139**, 87–99.
12. Paull,T.T. and Lee,J.H. (2005) The Mre11/Rad50/Nbs1 complex and its role as a DNA double-strand break sensor for ATM. *Cell cycle*, **4**, 737–740.
13. Zou,L. and Elledge,S.J. (2003) Sensing DNA damage through ATRIP recognition of RPA-ssDNA complexes. *Science*, **300**, 1542–1548.
14. Marechal,A. and Zou,L. (2015) RPA-coated single-stranded DNA as a platform for post-translational modifications in the DNA damage response. *Cell Res.*, **25**, 9–23.
15. Walker,J.R., Corpina,R.A. and Goldberg,J. (2001) Structure of the Ku heterodimer bound to DNA and its implications for double-strand break repair. *Nature*, **412**, 607–614.
16. Hammel,M., Yu,Y., Mahaney,B.L., Cai,B., Ye,R., Phipps,B.M., Rambo,R.P., Hura,G.L., Pelikan,M., So,S. *et al.* (2010) Ku and DNA-dependent protein kinase dynamic conformations and assembly regulate DNA binding and the initial non-homologous end joining complex. *J. Biol. Chem.*, **285**, 1414–1423.
17. Spagnolo,L., Rivera-Calzada,A., Pearl,L.H. and Llorca,O. (2006) Three-dimensional structure of the human DNA-PKcs/Ku70/Ku80 complex assembled on DNA and its implications for DNA DSB repair. *Mol. Cell*, **22**, 511–519.

18. Gottlieb,T.M. and Jackson,S.P. (1993) The DNA-dependent protein kinase: requirement for DNA ends and association with Ku antigen. *Cell*, **72**, 131–142.
19. Ochi,T., Blackford,A.N., Coates,J., Jhujh,S., Mehmood,S., Tamura,N., Travers,J., Wu,Q., Draviam,V.M., Robinson,C.V. *et al.* (2015) DNA repair. PAXX, a paralog of XRCC4 and XLF, interacts with Ku to promote DNA double-strand break repair. *Science*, **347**, 185–188.
20. Fattah,F., Lee,E.H., Weisensel,N., Wang,Y., Lichter,N. and Hendrickson,E.A. (2010) Ku regulates the non-homologous end joining pathway choice of DNA double-strand break repair in human somatic cells. *PLoS Genet.*, **6**, e1000855.
21. Boboila,C., Yan,C., Wesemann,D.R., Jankovic,M., Wang,J.H., Manis,J., Nussenzweig,A., Nussenzweig,M. and Alt,F.W. (2010) Alternative end-joining catalyzes class switch recombination in the absence of both Ku70 and DNA ligase 4. *J. Exp. Med.*, **207**, 417–427.
22. Mimori,T., Hardin,J.A. and Steitz,J.A. (1986) Characterization of the DNA-binding protein antigen Ku recognized by autoantibodies from patients with rheumatic disorders. *J. Biol. Chem.*, **261**, 2274–2278.
23. Caldecott,K.W. (2008) Single-strand break repair and genetic disease. *Nat. Rev. Genet.*, **9**, 619–631.
24. Liu,C., Vyas,A., Kassab,M.A., Singh,A.K. and Yu,X. (2017) The role of poly ADP-ribosylation in the first wave of DNA damage response. *Nucleic Acids Res.*, **45**, 8129–8141.
25. Ali,A.A.E., Timinszky,G., Arribas-Bosacoma,R., Kozlowski,M., Hassa,P.O., Hassler,M., Ladurner,A.G., Pearl,L.H. and Oliver,A.W. (2012) The zinc-finger domains of PARP1 cooperate to recognize DNA strand breaks. *Nat. Struct. Mol. Biol.*, **19**, 685–692.
26. Langelier,M.F. and Pascal,J.M. (2013) PARP-1 mechanism for coupling DNA damage detection to poly(ADP-ribose) synthesis. *Curr. Opin. Struct. Biol.*, **23**, 134–143.
27. Ludwig,A., Behnke,B., Holtlund,J. and Hilz,H. (1988) Immunoquantitation and size determination of intrinsic poly(ADP-ribose) polymerase from acid precipitates. An analysis of the in vivo status in mammalian species and in lower eukaryotes. *J. Biol. Chem.*, **263**, 6993–6999.
28. Yamanaka,H., Penning,C.A., Willis,E.H., Wasson,D.B. and Carson,D.A. (1988) Characterization of human poly(ADP-ribose) polymerase with autoantibodies. *J. Biol. Chem.*, **263**, 3879–3883.
29. Lautier,D., Lagueux,J., Thibodeau,J., Menard,L. and Poirier,G.G. (1993) Molecular and biochemical features of poly (Adp-ribose) metabolism. *Mol. Cell Biochem.*, **122**, 171–193.
30. Langelier,M.F., Planck,J.L., Roy,S. and Pascal,J.M. (2012) Structural basis for DNA damage-dependent poly(ADP-ribosyl)ation by human PARP-1. *Science*, **336**, 728–732.
31. Ray Chaudhuri,A. and Nussenzweig,A. (2017) The multifaceted roles of PARP1 in DNA repair and chromatin remodelling. *Nat. Rev. Mol. Cell Biol.*, **18**, 610–621.
32. Ahel,I., Ahel,D., Matsusaka,T., Clark,A.J., Pines,J., Boulton,S.J. and West,S.C. (2008) Poly(ADP-ribose)-binding zinc finger motifs in DNA repair/checkpoint proteins. *Nature*, **451**, 81–85.
33. Ahel,D., Horejsi,Z., Wiechens,N., Polo,S.E., Garcia-Wilson,E., Ahel,I., Flynn,H., Skehel,M., West,S.C., Jackson,S.P. *et al.* (2009) Poly(ADP-ribose)-dependent regulation of DNA repair by the chromatin remodeling enzyme ALC1. *Science*, **325**, 1240–1243.
34. Mao,Z., Hine,C., Tian,X., Van Meter,M., Au,M., Vaidya,A., Seluanov,A. and Gorbunova,V. (2011) SIRT6 promotes DNA repair under stress by activating PARP1. *Science*, **332**, 1443–1446.
35. Toiber,D., Erdel,F., Bouazoune,K., Silberman,D.M., Zhong,L., Mulligan,P., Sebastian,C., Cosentino,C., Martinez-Pastor,B., Giacosa,S. *et al.* (2013) SIRT6 recruits SNF2H to DNA break sites, preventing genomic instability through chromatin remodeling. *Mol. Cell*, **51**, 454–468.
36. Wu,L.E., Gomes,A.P. and Sinclair,D.A. (2014) Geroncogenesis: metabolic changes during aging as a driver of tumorigenesis. *Cancer Cell*, **25**, 12–19.
37. Wang,C., Chen,L., Hou,X., Li,Z., Kabra,N., Ma,Y., Nemoto,S., Finkel,T., Gu,W., Cress,W.D. *et al.* (2006) Interactions between E2F1 and SirT1 regulate apoptotic response to DNA damage. *Nat. Cell Biol.*, **8**, 1025–1031.
38. Wang,R.H., Sengupta,K., Li,C., Kim,H.S., Cao,L., Xiao,C., Kim,S., Xu,X., Zheng,Y., Chilton,B. *et al.* (2008) Impaired DNA damage response, genome instability, and tumorigenesis in SIRT1 mutant mice. *Cancer Cell*, **14**, 312–323.
39. Soutoglou,E., Dorn,J.F., Sengupta,K., Jasin,M., Nussenzweig,A., Ried,T., Danuser,G. and Misteli,T. (2007) Positional stability of single double-strand breaks in mammalian cells. *Nat. Cell Biol.*, **9**, 675–682.
40. Howard,S.M., Yanez,D.A. and Stark,J.M. (2015) DNA damage response factors from diverse pathways, including DNA crosslink repair, mediate alternative end joining. *PLoS Genet.*, **11**, e1004943.
41. Monteilhet,C., Perrin,A., Thierry,A., Colleaux,L. and Dujon,B. (1990) Purification and characterization of the in vitro activity of I-Sce I, a novel and highly specific endonuclease encoded by a group I intron. *Nucleic Acids Res.*, **18**, 1407–1413.
42. Vilenchik,M.M. and Knudson,A.G. (2003) Endogenous DNA double-strand breaks: Production, fidelity of repair, and induction of cancer. *Proc. Natl Acad. Sci. U.S.A.*, **100**, 12871–12876.
43. Wang,M.L., Wu,W.Z., Wu,W.Q., Rosidi,B., Zhang,L.H., Wang,H.C. and Iliakis,G. (2006) PARP-1 and Ku compete for repair of DNA double strand breaks by distinct NHEJ pathways. *Nucleic Acids Res.*, **34**, 6170–6182.
44. Paddock,M.N., Bauman,A.T., Higdon,R., Kolker,E., Takeda,S. and Scharenberg,A.M. (2011) Competition between PARP-1 and Ku70 control the decision between high-fidelity and mutagenic DNA repair. *DNA Repair*, **10**, 338–343.
45. Hochegger,H., Dejsuphong,D., Fukushima,T., Morrison,C., Sonoda,E., Schreiber,V., Zhao,G.Y., Saberi,A., Masutani,M., Adachi,N. *et al.* (2006) Parp-1 protects homologous recombination from interference by Ku and Ligase IV in vertebrate cells. *EMBO J.*, **25**, 1305–1314.
46. Fell,V.L. and Schild-Poulter,C. (2015) The Ku heterodimer: Function in DNA repair and beyond. *Mutat. Res.-Rev. Mutat.*, **763**, 15–29.
47. Hustedt,N. and Durocher,D. (2017) The control of DNA repair by the cell cycle. *Nat. Cell Biol.*, **19**, 1–9.
48. Dueva,R. and Iliakis,G. (2013) Alternative pathways of non-homologous end joining (NHEJ) in genomic instability and cancer. *Transl. Cancer Res.*, **2**, 163–177.
49. Ogata,N., Ueda,K., Kawaichi,M. and Hayaishi,O. (1981) Poly(Adp-ribose) synthetase, a main acceptor of poly(Adp-ribose) in isolated-nuclei. *J. Biol. Chem.*, **256**, 4135–4137.
50. Mortusewicz,O., Ame,J.C., Schreiber,V. and Leonhardt,H. (2007) Feedback-regulated poly(ADP-ribosyl)ation by PARP-1 is required for rapid response to DNA damage in living cells. *Nucleic Acids Res.*, **35**, 7665–7675.
51. Liu,C. and Yu,X.C. (2015) ADP-Ribosyltransferases and Poly ADP-ribosylation. *Curr. Protein Pept. Sci.*, **16**, 491–501.
52. McGowan,C.H. and Russell,P. (2004) The DNA damage response: sensing and signaling. *Curr. Opin. Cell Biol.*, **16**, 629–633.
53. Lamarche,B.J., Orazio,N.I. and Weitzman,M.D. (2010) The MRN complex in double-strand break repair and telomere maintenance. *FEBS Lett.*, **584**, 3682–3695.